Formation of local electric dipoles with no unique polar axis in $Tb_3Fe_5O_{12}$

Despina Louca,[1] K. Kamazawa,[1,*] and T. Proffen[2]
[1]*Department of Physics, University of Virginia, Charlottesville, Virginia 22904, USA*
[2]*Los Alamos National Laboratory, Los Alamos, New Mexico 87545, USA*
(Received 21 October 2008; revised manuscript received 6 November 2009; published 8 December 2009)

Using neutron scattering and the pair-density-function analysis, we investigated, the local atomic structure of the ferrimagnetic dielectric $Tb_3Fe_5O_{12}$ garnet. Pronounced magnetic diffuse scattering is observed at high temperatures that gradually decreases with cooling as the Tb spins take on an ordered structure at about 50 K. In the temperature range where the dielectric (ε) constant is enhanced, a volume striction is observed from the diffraction measurements under a magnetic field that couples the magnetic response to the dielectric properties. At the same time, large oxygen displacements, on the order of 0.1–0.2 Å, are observed starting first at 90 K that persist up to 550 K, resulting in the formation of electric dipoles. However, they are not ordered and the lack of a unique polar axis in the hyperkagome structure may be linked to the absence of a polarized phase in this system. If it were present, the system could have a high ferroelectric transition temperature.

DOI: 10.1103/PhysRevB.80.214406 PACS number(s): 61.05.F−, 75.25.+z, 75.50.Gg, 75.80.+q

I. INTRODUCTION

The resurgence of interest in recent years in materials that exhibit magnetoelectric (ME) coupling has been driven by the discovery of gigantic ME responses in oxides.[1–4] Although materials in which coexisting, and most likely competing, ferromagnetic or antiferromagnetic and ferroelectric or ferroelastic order parameters have been studied for decades, in some of the earlier systems investigated,[5,6] the ferroelectric transition appeared at a much higher temperature than the magnetic transition, thus the coupling between the two-order parameters was weak. However, in the newer multiferroic compounds, electric polarization coincides with a magnetic transition to a spiral phase[7,8] to produce a stronger effect. Magnetoelectricity may arise either by direct coupling between the magnetic and electric order parameters or indirectly through elastic strain.[9] Most real multiferroic materials have either small permittivity or permeability and their linear magnetoelectric coupling is also small. Indirect coupling through strain in the form of magnetostriction is equally important and may become dominant in some cases as it generates new interaction terms between the magnetic and electrical fields.[10]

The key to understanding the microscopic nature of the magnetoelectric behavior is in the crystal structure and magnetic symmetries. Small changes in the symmetry of the crystal may enhance or eliminate the ME effect.[11,12] In this paper, we focus on one system, the ferrimagnetic garnet $Tb_3Fe_5O_{12}$ that shows evidence of coupling via the field-induced changes in the dielectric constant, ε,[13] but with no spontaneous polarization. The changes in ε are observed in a temperature range where several other transitions are expected to take place: earlier studies suggested that the Tb spins form a modulated magnetic structure in the already ordered magnetic state of the Fe sublattice with cooling, while the crystal symmetry changes from cubic to rhombohedral.[14–19] Thus, on revisiting this system, we want to examine in detail the nature of the structural distortions associated with the dielectric phase as well as the dynamics accompanying the magnetic transition of the Tb sublattice.

When a rare-earth magnetic ion occupies the C site of a garnet crystal with the $C_3A_2D_3O_{12}$ chemical formula, while the A and D sites are occupied by nonmagnetic ions, long-range antiferromagnetic ordering may occur as in $Tb_3Ga_5O_{12}$ (Ref. 20) and $Dy_3Al_5O_{12}$,[21] typically at temperatures much lower than the Curie-Weiss, θ_C, temperature, due to the presence of underlying competing interactions. Certain notable exceptions include $Gd_3Ga_5O_{12}$ (Ref. 22) where the triangular arrangement of the Gd spins at the C site frustrates the system magnetically and nearest neighbor interactions alone are not sufficient to induce a magnetic transition at any temperature. If the A and D sites are occupied by magnetic ions such as a transition metal, frustration is suppressed and a long-range magnetic transition is observed as in $Tb_3Fe_5O_{12}$ or $Y_3Fe_5O_{12}$. In this case, a ferrimagnetic transition occurs at relatively high temperatures, ~550 K, and is attributed to the antiferromagnetic ordering of Fe at the A sublattice with a multiplicity of 16 and the D sublattice with a multiplicity of 24 (J_{AD} between A and D is large and negative where J is the coupling constant). The Tb spins at the C site with a multiplicity of 24 are thought to align antiparallel to the net magnetic Fe moment (J_{CD} and J_{CA} between C and A/D are also large and negative). The Tb moments align along the [111] direction which is the anisotropy axis in this crystal. All other interactions such as J_{AA}, J_{DD}, and J_{CC} are estimated to be much weaker.[19] At ~250 K, a compensation point is reached between the Tb and Fe spins where the bulk magnetization goes to zero as the Tb and Fe moments cancel each other out as seen in Fig. 1 (Ref. 23) which is a plot of the bulk susceptibility, χ, versus temperature. While the Fe moments are collinear to the (111) direction, the Tb spins form a modulated structure with cooling which is a conical spiral with an axis centered along (111). The Tb spin canting appears to slow down by ~50 K (Ref. 18) at which temperature the Tb spins arrange themselves in a new magnetic structure which takes on a rhombohedral symmetry. Simultaneously, the crystal symmetry transforms as well from cubic to rhombohedral. Around 150 K, ε is enhanced with cooling in the presence of a magnetic field, less than 0.2 T.[13] The field required to induce the change is significantly smaller than what it takes for the other multiferroics, i.e.,

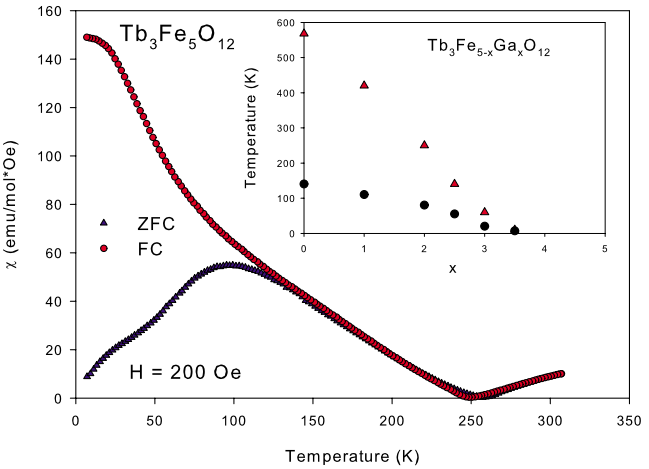

FIG. 1. (Color online) The FC and ZFC bulk magnetic susceptibilities, χ, at 200 Oe. The ferrimagnetic transition, T_N, is at ~550 K. A compensation point is reached at 250 K. On cooling, the ZFC and FC curves start to split, ~140 K. (Inset) The temperature dependence of T_N and T_{SG}. When Ga is substituted for Fe, T_N is suppressed down to zero and so is the split between FC and ZFC.

$TbMnO_3$, and could in principle be very useful in device applications combined with the fact that $Tb_3Fe_5O_{12}$ is insulating. The magnetodielectric response has been associated with the large magnetostriction correlated with the rhombohedral transition.

To address the origin of the magnetodielectric response in $Tb_3Fe_5O_{12}$, the relation of ε to the structural and magnetic transitions needs to be explored. To do so, we will address three issues in this paper. (1) As earlier studies suggested, the magnetic structure involving the Tb spins that forms upon cooling is conical. Is this sufficient to make the system polar? The conical magnetic structure is noncollinear in which a ferromagnetic component coexists with a screw or with a cycloidal spiral structure.[24] While inversion symmetry is broken it may not be sufficient to make the system polar without a magnetic field as in cycloidal spiral magnet of $TbMnO_3$.[25] Thus from this point of view, the dielectric response may not be related to the magnetic transition. (2) At the temperature where the dielectric response is observed, a lattice distortion occurs as well. Does the new lattice structure break spatial inversion symmetry? The $R\bar{3}c$ symmetry reached with cooling is centrosymmetric,[26] just like the high-temperature cubic, $Ia\bar{3}d$ symmetry, however. (3) Is the change in the lattice volume, magnetovolume striction, the driving force for the dielectric effect?

The present work gives the following results. With the use of high-resolution neutron diffraction, the pair-density-function (PDF) analysis and inelastic scattering, we determined that the lattice volume changes with field and this may be linked to the magnetodielectric response. The volume striction is most pronounced at low temperatures and coincides with the largest response in ε. Pronounced magnetic diffuse scattering is observed starting from high temperatures that gradually decreases with cooling. Spin freezing is observed at an energy transfer of $E=0$ meV at 50 K which coincides with the temperature at which the Tb structure forms. At higher energy transfers, spins appear to fluctuate at higher temperatures. At the same time, large oxygen displacements (~0.1–0.2 Å) coupled with the Tb and Fe ions have the opposite trend with temperature, namely they appear starting ~90 K and higher indicating that electric dipoles are indeed present. It is interesting to note that the distortions do not occur in the temperature range where ε changes. The displacements are *not ordered* and lack a unique polar axis in the hyperkagome structure that is linked to the absence of a polarized phase in this system. Thus, the magnetic transition does not coincide with the dielectric transition and most likely has little or no influence on the dielectric response. At the same time, the change in the dielectric function is most likely enhanced by the volume striction observed with lowering the temperature and increasing magnetic field. In addition, the absence of a polar axis may explain why this system is not ferroelectric at high temperatures in spite of the fact that local oxygen displacements are present.

II. EXPERIMENTAL

The powder sample of $Tb_3Fe_5O_{12}$ was prepared by standard solid-state reaction. The characterization of the bulk magnetization, χ, shows a difference in the zero-field-cooled (ZFC) and field-cooled (FC) dependences of the susceptibility as seen in Fig. 1. The higher transition temperature, T_N, is not shown in this figure. With cooling, the FC curve continuous to rise until it saturates while the ZFC curve turns downwards toward zero at around 140 K indicating a spin-glass transition, T_{SG}. Shown in the inset of Fig. 1 is the effects of Ga substitution at the Fe site, $Tb_3Fe_{5-x}Ga_xO_{12}$, on T_N, and T_{SG}. At $x=0$, no Ga, T_N is maximum, at ~550 K. At the same time, T_{SG} is also highest at ~140 K. T_N is suppressed by doping with Ga because Ga preferentially occupies the A sites and when the A site is mostly Ga as when $x\sim3$, no transition is observed. The Néel transition temperature varies almost identically with composition as in other garnets such as $Y_3Fe_5O_{12}$ (Refs. 27 and 28) indicating that the ordering of spins at the A and D sites is independent of the kind of rare-earth ion residing at the C site. At the same time, by suppressing T_N with increasing Ga doping, the cusp observed in the ZFC curve of Fig. 1 shifts to lower temperatures and eventually disappears which suggests that the Tb and Fe spin exchange interactions are important in driving the formation of a Tb modulated structure.

The neutron diffraction measurements were performed as a function of temperature at NPDF of Los Alamos National Laboratory without field and at GPPD of Argonne National Laboratory with field, using an electromagnet attached to the closed-cycle refrigeration system where a maximum field of 1 tesla (T) could be reached. The inelastic measurements were performed at SPINS, the cold triple-axes spectrometer at the NIST Center for Neutron Research. The diffraction data were analyzed using the Rietveld refinement performed in reciprocal space and the PDF analysis in real space. The Rietveld refinement provides a description of the average or long-range atomic arrangement, with reliable information of the unit-cell parameters and average atomic coordinates,

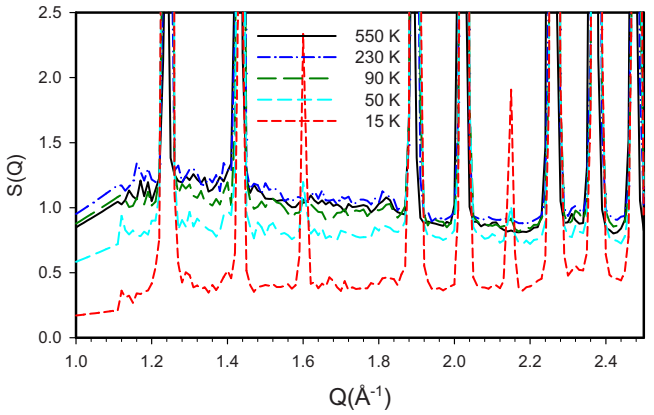

FIG. 2. (Color online) The temperature dependence of the structure function, $S(Q)$, as a function of momentum transfer, Q. Diffuse scattering that appears as background (different from instrumental background) is observed starting at 550 K, with little or no change with cooling down to 90 K. Below this temperature, the background is reduced by 50 K, magnetic Bragg peaks appear. By 15 K, the magnetic Bragg peaks become stronger where little or no diffuse scattering is present.

while the PDF provides us with information on local distortions that do not follow the lattice periodicity.

III. RESULTS AND CONCLUSION

Shown in Fig. 2 is the structure function, $S(Q)$, where Q is the momentum transfer, determined from the diffraction data collected at the NPDF instrument. The $S(Q)$ is evaluated at several temperature points as data were collected from 550 down to 15 K. Starting from the highest temperature, diffuse scattering is evident in the $S(Q)$ as the function rises at low Q in spite of subtracting the instrumental background from the data. The origin of the diffuse scattering is magnetic, centered around low Q. It arises from the randomness of the Tb moments and its dependence on Q follows the Tb form factor. The presence of magnetic diffuse scattering is consistent with earlier reports that proposed that not all Tb moments align with the Fe moments along the (111) direction at high temperatures. With cooling, the diffuse scattering changes very slowly until about 90 K. Between 90 and 50 K, the diffraction pattern shows a marked drop in the background. This coincides with the Tb spin alignment. By 15 K, the diffuse scattering is reduced to a minimum and the magnetic structure is fully formed with the magnetic peaks becoming Bragg-type although significantly smaller than the nuclear Bragg peaks. A plot of the magnetic peak intensity at $Q=1.6$ Å^{-1} as a function of temperature is shown in Fig. 3(a). The intensity increases dramatically below 50 K which corresponds to the magnetic transition of the Tb moments.

The origin of the diffuse scattering is explored further by investigating how the low-Q magnetic intensity fluctuates with energy at one Q value of $Q=1.1$ Å^{-1}. Data were collected at five different temperatures with a fixed $E_f=2.5$ meV at SPINS using a conventional analyzer and Be and BeO filters used in the incident and scattered beams, respectively, to eliminate $\lambda/2$ contamination and are plotted

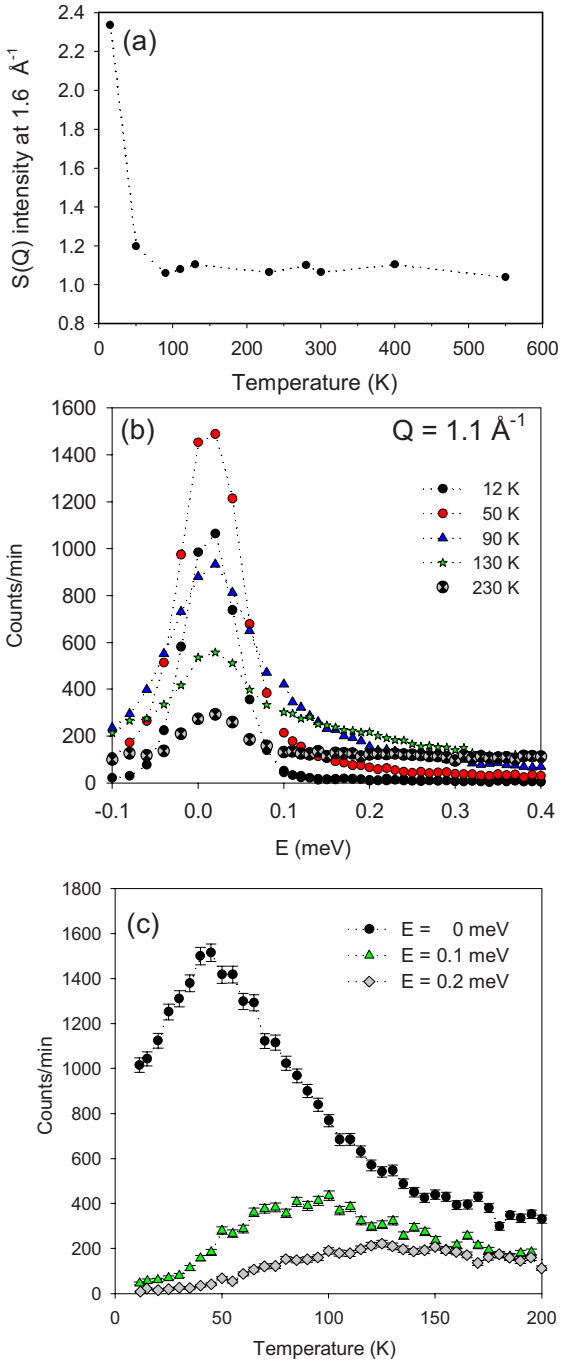

FIG. 3. (Color online) (a) A plot of the intensity at 1.6 Å^{-1} Bragg peak as a function of temperature. The intensity increases at the magnetic transition of 50 K. (b) The inelastic intensity as a function of temperature at $Q=1.1$ Å^{-1}. The scattering intensity is centered around $E=0$ meV and increases with cooling. By ~50 K, it reaches a maximum and then decreases with further cooling. (c) The intensity measured at three constant energy transfers. At $E=0$ meV, a maximum is reached at 50 K, which corresponds to the intensity reaching a maximum of Fig. 3(a). At higher energy transfers, the maximum shifts to higher temperatures and becomes broad. Thus 50 K corresponds to the characteristic temperature of spin freezing. This temperature coincides with the magnetic transition temperature. At the same time, spins weakly fluctuate at higher temperatures.

TABLE I. The results of the Rietveld refinement using the high-temperature $Ia\bar{3}d$ symmetry and the low-temperature $R\bar{3}c$ symmetry. In the $Ia\bar{3}d$ symmetry from 550 to 130 K, Tb is at (1/8, 0, 1/4), Fe at (0, 0, 0) and (3/8, 0, 1/4), and O at (x,y,z). In the $R\bar{3}c$ symmetry from 130 down to 10 K, Tb is at (~0.626, 0, 1/4) and (~0.126, 0, 1/4), Fe at (0, 0, 0), (1/2, 0, 0), and (~0.209, ~0.169, ~0.413). The oxygen coordinates along with the lattice constants are listed below.

Symmetry	Parameters
$Ia\bar{3}d$	$a=12.4338$ (±0.0003) (Å)
	$x_O=-0.0276$, $y_O=0.0557$, $z_O=0.1501$
$R\bar{3}c$	$a=17.5645$ (±0.0005) (Å), $c=10.7555$
	$x_O=0.3357$, $y_O=0.5789$, $z_O=0.7876$
	$x_O=0.7626$, $y_O=0.8214$, $z_O=0.4165$
	$x_O=0.7581$, $y_O=0.7154$, $z_O=0.6215$
	$x_O=0.1462$, $y_O=0.8857$, $z_O=0.1733$

as a function of energy. From this measurement it is clear that the origin of the diffuse scattering observed in the $S(Q)$ of Fig. 1 is quasielastic, centered around the elastic peak of $E=0$ meV [Fig. 3(b)]. With cooling, the intensity of the central peak is enhanced and reaches a maximum by 50 K but then comes down by 12 K, indicating that the inelastic intensity reaches a maximum at 50 K that is he magnetic transition temperature determined in Fig. 3(a). The magnetic fluctuations giving rise to the quasielastic intensity diminish with the transition. In Fig. 3(c), three constant energy scans are shown as a function of temperature. At $E=0$ meV, the elastic order parameter shows a characteristic temperature of ~45 K. This temperature corresponds to the spin-freezing temperature and coincides with the appearance of the Bragg peaks in the structure factor and the reduction in the diffuse scattering. At $E=0.1$ meV, the characteristic temperature shifts to higher values (~85 K) and the intensity weakens significantly. At an even higher energy transfer, $E=0.2$ meV, the intensity is very weak and the characteristic temperature of the fluctuations becomes very broad. Thus spin fluctuations are prevalent at temperatures between 50 and 200 K, the maximum temperature reached during this experiment. The characteristic energy of these fluctuations varies with temperature, with higher energy fluctuations present at higher temperatures that gradually disappear with the spin freezing.

The diffraction data were also collected as a function of field using the 1 T electromagnet. The results from the Rietveld refinement are summarized in Table I. Shown in the table are the crystal structure parameters for the cubic, $Ia\bar{3}d$ phase obtained at room temperature and for the rhombohedral phase, $R\bar{3}c$, at 90 K at zero field. Since the dielectric constant was previously shown to change at very small fields, *less* than 0.2 T,[13] the 1 T electromagnet was sufficient to investigate the structural changes within the field range in question. The $R\bar{3}c$ phase was also used to refine the data with field. From the refinement, the unit-cell volume is extracted and its change with field and temperature is summarized in Table II. We find that volume striction is enhanced with field particularly below 90 K. These changes are consistent with the field-induced enhancement of ε and may be the driving force for the field dependence on ε. Thus the ME coupling in this system is mediated via the elastic strain induced by striction. At a microscopic level, an important ingredient to magnetostriction is spin-orbit coupling as well as coupling of the orbital to the lattice degree of freedom. The $4f$ electrons of Tb posses both spin and orbital angular momenta and due to crystal electric fields, the electronic charge distribution may become very anisotropic.[18] When the magnetic field is turned on, the ionic cloud follows and distorts the lattice. Such internal magnetoelastic strain develops under orbital angular momentum rotations. From the results presented thus far, it is evident that the transition of the Tb magnetic structure is not directly related to the changes in ε. ε starts to change with temperature below 150 K, while the Tb magnetic transition occurs at around 50 K.

TABLE II. The change in the unit-cell volume as a function of field at constant temperature scans. The volume decreases with increasing field due to magnetostriction.

Temperature (K)	Magnetic Field (Oe)	Volume (Å^3)
15	0	1910.9990
	2000	1907.5130
	7000	1906.5880
90	0	1913.0710
	2000	1910.4830
	7000	1910.3380
130	0	1914.1950
	2000	1911.9490
	7000	1911.8820

The $Tb_3Fe_5O_{12}$ garnet does not become polar like the other multiferroic systems for reasons that can be understood by looking at the local atomic structure. The local structure analysis was performed by Fourier transforming the $S(Q)$ of Fig. 2 and the results show evidence for large oxygen distortions, particularly with increasing the temperature. This is quite surprising considering that no polarization has been measured in this system. Starting from the lowest temperature, 15 K, the PDF obtained by Fourier transforming the $S(Q)$ in real space is compared to a model PDF (solid line) calculated based on the crystallographic symmetry [Fig. 4(a)]. Overall, the two are in very good agreement. From the model the partial PDF's can be readily determined and these are also plotted in the figure as well. The partials for the different pairs help identify the peaks in real space. For instance, the first two peaks correspond to one tetrahedral and two octahedral Fe-O correlations: the tetrahedral bonds range from 1.83–1.97 Å, and the octahedral bonds inside the cell range from 1.97–2.06 Å and at the corners of the unit cell at 2.09 Å. The second peak corresponds to Tb-O correlations. Following are O-O correlations, Tb-Fe, Fe-Fe, and Tb-Tb pairs. Shown in Fig. 3(b) is the temperature dependence of the PDF in an expanded region that includes only the Fe-O

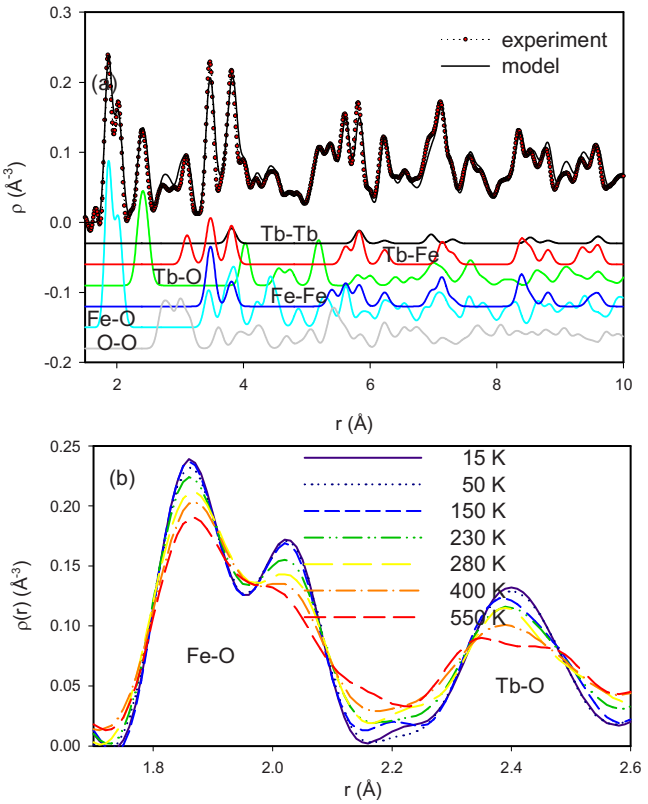

FIG. 4. (Color online) (a) A comparison of the PDF determined from data collected at 15 K (symbols) with a model PDF (solid line) calculated assuming the crystal model at 300 K. Also shown are the partial PDF's corresponding to the different pairs of atoms. (b) The PDF's are plotted in an expanded range that includes the Fe-O and Tb-O peaks only as a function of temperature.

and Tb-O bond correlations. Interestingly, starting from the lowest temperature, only one local Tb-O bond and two Fe-O bonds are present although the widths of these peaks are quite broad and include a range of bonds. As the temperature increases, two distinct types of Tb-O and three Fe-O bonds are observed starting from about 100 K. This finding shows that although the structure is cubic on average from 150–550 K, locally the symmetry is broken, allowing for more than one Tb-O bond. Similarly, the Fe-O peak corresponding to the octahedral bonds splits as well and follows the temperature dependence of the Tb-O bonds. This can be seen in Fig. 5 which is a plot of the bond lengths as a function of temperature. The Fe-O octahedra expand by about 0.2 Å while the Tb-O triangular sites expand by 0.1 Å. These displacements are sizeable in comparison to what has been observed in other multiferroics[29] and one could expect the system to show a degree of polarization.

IV. DISCUSSION

The key to understanding the absence of polarization lies in the nature of the distortions and how they are organized in the long-range structure. For this, the central atom is oxygen. The oxygen ion is a bridge ion between the Tb triangular and Fe octahedral sites, and the movement of oxygen indicates

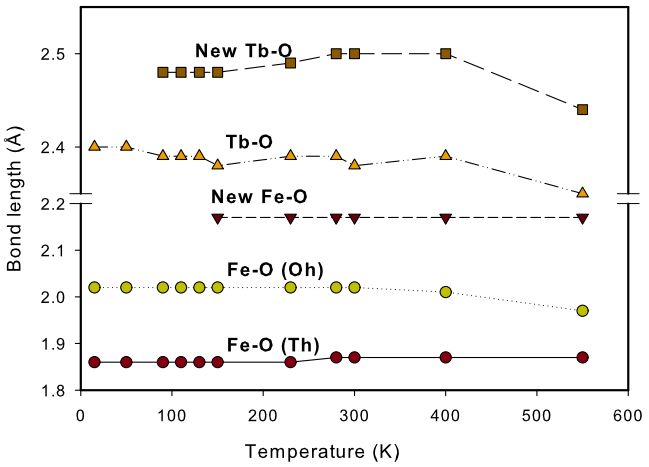

FIG. 5. (Color online) The temperature dependence of the Tb-O and Fe-O bond lengths. According to the cubic symmetry, only two Fe-O bonds and one Tb-O bond should be present, but locally, there are three Fe-O and two Tb-O bonds starting at ~90 all the way to 550 K.

the presence of possible electric dipoles with increasing temperature. The fact that two Tb-O and three Fe-O distinct groups of bonds are found in the local structure particularly at elevated temperatures is in contrast to the cubic symmetry that fits the diffraction data well at elevated temperatures. This means that locally, the cubic symmetry is broken but the distortions are randomized. One likely scenario that can explain these results is to consider the complexity of the hyperkagome garnet structure and the possibility that no unique polar axis can easily form with the displacements of oxygen. Oxygen distortions occur in the three-dimensional network in a random fashion and do not allow for electric polarization of this system. In this case it is the coordinated motion of the oxygen ions that is crucial to producing a unique polar axis in this system. To conclude, the structural and magnetic transitions observed in this system do not appear to be directly related to the magnetodielectric response. Instead, the field-induced enhancement of ε is strongly linked with the magnetovolume striction that may in turn be associated with the Tb orbital angular momentum rotations.

ACKNOWLEDGMENTS

The authors would like to acknowledge the help of the late Jim Richardson during the GPPD experiment and D. Phelan during the SPINS measurements. Work at the University of Virginia is supported by the U.S. Department of Energy under Contract No. DE-FG02-01ER45927. This work has benefited from the use of NPDF at the Lujan Center at Los Alamos Neutron Science Center, funded by DOE Office of Basic Energy Sciences. Los Alamos National Laboratory is operated by Los Alamos National Security LLC through DOE under Contract No. DE-AC52-06NA25396.

*Present address: Toyota Central R&D Labs. Inc., Nagakute, Aichi 480-1192, Japan.

[1] T. Kimura, T. Goto, H. Shintani, K. Ishizaka, T. Arima, and T. Tokura, Nature (London) **426**, 55 (2003).

[2] N. Hur, S. Park, P. A. Sharma, J. S. Ahn, S. Guha, and S.-W. Cheong, Nature (London) **429**, 392 (2004).

[3] B. Lorenz, A. P. Litvinchuk, M. M. Gospodinov, and C. W. Chu, Phys. Rev. Lett. **92**, 087204 (2004).

[4] T. Lottermoser and M. Fiebig, Phys. Rev. B **70**, 220407(R) (2004).

[5] G. A. Smolenskii, A. I. Agranovskaya, S. N. Popov, and V. A. Isupov, Usp. Fiziol. Nauk **28**, 2152 (1958).

[6] E. Ascher, H. Rieder, H. Schmid, and H. Stössel, J. Appl. Phys. **37**, 1404 (1966).

[7] M. Kenzelmann, A. B. Harris, S. Jonas, C. Broholm, J. Schefer, S. B. Kim, C. L. Zhang, S.-W. Cheong, O. P. Vajk, and J. W. Lynn, Phys. Rev. Lett. **95**, 087206 (2005).

[8] M. Mostovoy, Phys. Rev. Lett. **96**, 067601 (2006).

[9] W. Eerenstein, N. D. Mathur, and J. F. Scott, Nature (London) **442**, 759 (2006).

[10] N. A. Hill, J. Phys. Chem. B **104**, 6694 (2000).

[11] S. Takano, E. Kita, K. Siratori, K. Kohn, S. Kimura, and A. Tasaki, Ferroelectrics **162**, 73 (1994).

[12] Z. G. Ye, O. Crottaz, F. Vaudano, F. Kuber, and P. Tissot, Ferroelectrics **162**, 103 (1994).

[13] N. Hur, S. Park, S. Guha, A. Borissov, V. Kiryukhin, and S.-W. Cheong, Appl. Phys. Lett. **87**, 042901 (2005).

[14] M. Guillot and H. Legall, J. Phys. (France) **38**, 871 (1977).

[15] F. Tcheou, H. Fuess, and E. F. Bertaut, Solid State Commun. **8**, 1745 (1970).

[16] M. Lahoubi, M. Guillot, A. Marchand, F. Tcheou, and E. Roudaut, IEEE Trans. Magn. **20**, 1518 (1984).

[17] F. Sayetat, J. Appl. Phys. **46**, 3619 (1975).

[18] F. Sayetat, J. X. Boucherle, and F. Tcheou, J. Magn. Magn. Mater. **46**, 219 (1984).

[19] F. Sayetat, J. Magn. Magn. Mater. **58**, 334 (1986).

[20] K. Kamazawa, D. Louca, R. Morinaga, T. J. Sato, Q. Huang, J. R. D. Copley, and Y. Qiu, Phys. Rev. B **78**, 064412 (2008).

[21] B. E. Keen, D. P. Landau, and W. P. Wolf, Phys. Lett. **23**, 202 (1966).

[22] P. Schiffer, A. P. Ramirez, D. A. Huse, P. L. Gammel, U. Yaron, D. J. Bishop, and A. J. Valentino, Phys. Rev. Lett. **74**, 2379 (1995).

[23] D. Rodić, Z. Tomkowicz, L. Novaković, A. Szytula, and M. Lj. Napijalo, Solid State Commun. **73**, 243 (1990).

[24] D. E. Cox, W. J. Takei, and G. Shirane, J. Phys. Chem. Solids **24**, 405 (1963).

[25] T. Kimura, Annu. Rev. Mater. Res. **37**, 387 (2007).

[26] H. Hauptman and J. Karle, Acta Crystallogr. **12**, 1950 (1959).

[27] P. Hansen, J. Appl. Phys. **45**, 3638 (1974).

[28] M. Bonnet, A. Delapalme, H. Fuess, and P. Becker, J. Phys. Chem. Solids **40**, 863 (1979).

[29] S. Lee, A. Pirogov, M. Kang, K.-H. Jang, Y. Yonemura, T. Kamiyama, S.-W. Cheong, F. Gozzo, N. Shin, H. Kimura, Y. Noda, and J.-G. Park, Nature (London) **451**, 805 (2008).